Imaging human connectomes at the macroscale

R Cameron Craddock[1,2], Saad Jbabdi[3,9], Chao-Gan Yan[1,2,4,9], Joshua T Vogelstein[1,5–7], F Xavier Castellanos[2,4], Adriana Di Martino[4], Clare Kelly[4], Keith Heberlein[8], Stan Colcombe[2] & Michael P Milham[1,2]

At macroscopic scales, the human connectome comprises anatomically distinct brain areas, the structural pathways connecting them and their functional interactions. Annotation of phenotypic associations with variation in the connectome and cataloging of neurophenotypes promise to transform our understanding of the human brain. In this Review, we provide a survey of magnetic resonance imaging–based measurements of functional and structural connectivity. We highlight emerging areas of development and inquiry and emphasize the importance of integrating structural and functional perspectives on brain architecture.

First introduced in 2005 (ref. 1), the term 'connectome' embodies the advances of over a century of neuroscientific innovation and reflects an agenda for a new era. Initially defined as a complete map of neural connections in the brain, the connectome is a multiscale construct that can be examined at varying resolutions. At the extremes are the microscale, which encompasses individual neurons and their synaptic connections, and the macroscale, which encompasses cortical tissues (commonly a cubic centimeter or larger). The intermediate resolution is the mesoscale, which, in humans, encompasses vertical columns of 80–120 neurons (commonly referred to as micro- or mini-columns)[1,2]. Although all scales of resolution are intimately associated, each provides unique perspectives on the connectome. At the macroscale, and particularly in studies of the human brain, conceptualizations of the connectome have grown to also include information about function[3]. In this Review, we will use the term connectome to refer to brain areas, their anatomical connections and their functional interactions.

At present, methodologies for analysis at macroscale resolution are best positioned for mapping and annotating human connectomes with cognitive and behavioral associations. The higher-order, albeit lower-resolution, representations captured at the macroscale most directly relate to regulatory, cognitive and affective processes. Interpretation of macroscale-resolution findings is most amenable to guidance from lesion and brain-imaging studies. Comprehensive mapping and annotation of the connectome is most feasible at the lower-resolution macroscale, owing to lower computational and analytical demands. Moreover, noninvasive tools for *in vivo* imaging the human connectome are only available for analyses at the macroscale; *in vivo* microscale-resolution studies are currently limited to model organisms and neurosurgical patients.

Among the modalities used for macroconnectomics, magnetic resonance imaging (MRI) is dominant, partly because of widespread availability, safety and spatial resolution. Diffusion-weighted MRI (dMRI) and functional MRI (fMRI) are widely used for inferring structural and functional connectivity, respectively[4]. dMRI provides cubic-millimeter-resolution portrayals of white-matter tracts and insights into organizing principles that guide their orientation and

[1]Center for the Developing Brain, Child Mind Institute, New York, New York, USA. [2]Nathan Kline Institute for Psychiatric Research, Orangeburg, New York, USA. [3]The Oxford Centre for Functional MRI of the Brain, University of Oxford, Oxford, UK. [4]The Phyllis Green and Randolph Cowen Institute for Pediatric Neuroscience, Child Study Center, New York University Langone Medical Center, New York, New York, USA. [5]Department of Statistical Science, Duke University, Durham, North Carolina, USA. [6]Institute for Brain Sciences, Duke University, Durham, North Carolina, USA. [7]Institute for Data Intensive Engineering and Sciences, John Hopkins University, Baltimore, Maryland, USA. [8]Siemens Medical Solutions USA, Charlestown, Massachusetts, USA. [9]These authors contributed equally to this work. Correspondence should be addressed to S.C. (scolcombe@nki.rfmh.org) or M.P.M. (michael.milham@childmind.org).

RECEIVED 22 FEBRUARY; ACCEPTED 22 APRIL; PUBLISHED ONLINE 30 MAY 2013; DOI:10.1038/NMETH.2482

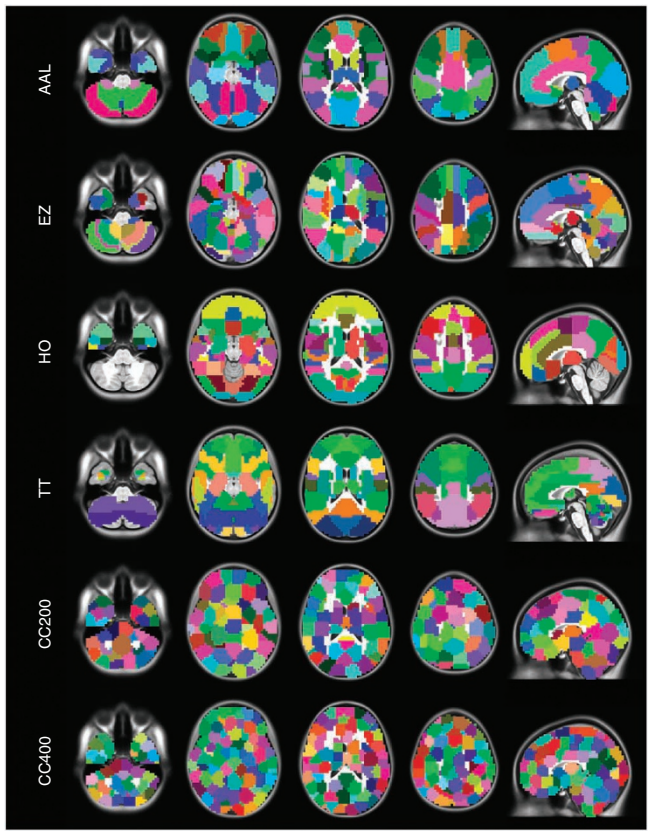

Figure 1 | Different parcellations of the human brain. Atlases of brain areas generated using anatomical (top four rows) and functional (bottom two rows) parcellation schemes show a lateral view (right) and top views of the human brain. AAL (automated anatomical labeling)[109] and Harvard Oxford (HO)[110] are derived from anatomical landmarks (sulci and gyral). The EZ (Eickhoff–Zilles)[111] and TT (Talariach Daemon)[112] atlases are derived from postmortem cyto- and myelo-architectonic segmentations. The CC200 and CC400 atlases are derived from 200- and 400-unit functional parcellations[11].

trajectories; fMRI reveals a universal functional architecture, with variations among individuals meaningfully related to phenotypic variables[5] (for example, behavioral and psychiatric).

In this Review, we focus on the mapping, characterization and analysis of macroscale connectomes. We structured our presentation in terms of a mathematical perspective that treats the connectome as a graph of interactions among brain areas. Nodes in the graph are abstract representations of brain areas, and edges represent pairwise relationships between nodes. We first review approaches and challenges to subdividing the brain into discrete subunits represented by nodes (here referred to as 'parcellation' efforts) and then review the imaging and analytic methodologies used to map and quantify patterns of structural and functional connectivity that are represented by edges in the connectome.

Defining nodes

Defining the nodes of a macroscale connectome is a complex task as we lack agreement on how best to define the constituent brain units. Depending on the scope of the investigation, the specific brain subunits represented by nodes can range from the small patches of cortex contained in individual MRI voxels to larger brain areas (for example, dorsolateral prefrontal cortex). Early parcellation efforts used postmortem architectonic measurements (for example, cell morphology) of single individuals. Although these resulting atlases are central to neuroscience, no functional or structural connectivity–based information was used to construct them, thus limiting their capacity to accurately represent connectomes. For example, despite being represented as a single area in anatomical atlases[6], the anterior cingulate region contains subregions that are each characterized by dramatically different functional[7] and structural[8] connectivity patterns. Although the large-scale human brain patterns captured using different strategies of parceling data may bear a gross similarity to one another, the specific details conveyed vary substantially (**Fig. 1**).

Ideally, both brain-function and structural-connectivity information should be used to delineate brain areas. Meta-analytic approaches can be used to define nodes on the basis of task-based fMRI (T-fMRI) studies[9]. Alternatively, data-driven clustering techniques can be used to subdivide the brain into areas based on homogeneity of functional time series[10,11], or functional or structural connectivity profiles[8,11,12]. Blinded source-separation techniques can also be used to define network nodes using spatial independence[13]. These methods commonly involve pooling of information across individuals, and most enforce specific properties on resulting brain areas[11]. One drawback is the need to prespecify the number of areas to be generated, which can be estimated based on homogeneity, accuracy, reproducibility or stability of the brain areas[10,11]. Optimal comparison of connectomes is likely to require parcellation strategies that incorporate information across individuals and modalities, potentially at the cost of quality of fit for single subjects and modalities.

Estimating structural connectivity

Structural connectivity encompasses the collection of axonal and dendritic connections among neurons[1]. Despite definitional simplicity, structural connectivity is difficult to measure with noninvasive, *in vivo* imaging approaches. Before dMRI, our knowledge was primarily derived from lesions and blunt dissection in humans or invasive tracing in nonhumans. These methodologies remain the gold standard for establishing connectivity, but the noninvasive nature of dMRI makes it the *de facto* standard for studies of human structural connectivity.

Acquisition. The basic principle underlying the inference of structural connectivity from dMRI data is that water diffusion in white matter is hindered and occurs primarily along the path of axons. In contrast, water diffusion in gray matter and cerebral spinal fluid occurs (almost) equally in all directions. By following the motion of water, it is possible to map the orientation(s) of fibers passing through each voxel of white matter. In dMRI, a series of images are acquired, each sensitive to diffusion along a specific direction. The number of images for unique directions acquired varies from six to hundreds. When combined, these images contain the information necessary to estimate the orientation(s) of fibers passing through each voxel; this information is used to reconstruct large-scale tracts of white matter (tractography). We describe dMRI acquisition in more detail in **Box 1** and **Table 1**.

BOX 1 OPTIMIZING fMRI AND dMRI IMAGE ACQUISITION

Echo-planar imaging (EPI) is the most common method for acquiring functional magnetic resonance imaging (fMRI) and diffusion MRI (dMRI) data. An EPI volume is a set of slices, each acquired after a single excitation. EPI volumes are collected in sequence, representing time points in fMRI data and diffusion directions in dMRI data. Gradient echo EPI in fMRI only involves excitation and readout. However, in dMRI an additional 180° rephasing (spin echo) radiofrequency pulse and bipolar diffusion–encoding gradients are applied.

$$\mathrm{SNR} \propto I_0 \times \Delta_x \times \Delta_y \times \Delta_z \times \sqrt{N_{acq} \times N_x \times N_y \times N_z \times \frac{1}{P_f}} \quad (1)$$

Signal-to-noise ratio (SNR), spatial distortions and artifacts, and image contrast determine image quality. Image SNR can be represented in terms of parameters such as available signal (I_0), voxel dimensions (Δ_x, Δ_y, Δ_z), number of image acquisitions (N_{acq}), number of samples in each dimension (N_x, N_y, N_z), time between samples (Δt) and parallel imaging factor (P_f) (equation (1))[117]. These parameters are described in **Table 1**. Equation (1) demonstrates how different parameter settings affect the SNR; for example, acquiring and averaging two volumes ($N_{acq} = 2$) improves SNR by $\sqrt{2}$. SNR for modern imaging technology is greater than required for most imaging applications and can be traded-off to optimize other imaging aspects (for example, to reduce spatial distortions). Beyond spatial image considerations, parameter optimizations must be evaluated in terms of impact on the temporal signal in fMRI or diffusion signal in dMRI.

General considerations for EPI

Spatial distortion. The EPI readout scheme leads to extended readout times and asymmetric bandwidth between directions that result in prolonged spin-spin (T2) relaxation, which increases in-plane smoothing. Bandwidth corresponds to the number of frequencies allocated to a voxel; any shift in frequency resulting from magnetic field imperfections spatially shifts the signal in proportion to the inverse of the bandwidth[118]. The bandwidth in the phase-encoding direction is a fraction of the bandwidth in the readout direction, making it particularly susceptible to spatial distortions. Increasing bandwidth can minimize spatial distortions, though costing SNR. Parallel imaging techniques increase effective bandwidth and image acquisition rate[119]. These techniques require calibration scans for proper reconstruction, and any misalignment (for example, head motion) between these scans and image data produce reconstruction errors[119]. Alternatively, spatial distortions can be mathematically corrected using maps of the spatial variation in the magnetic field[15].

Image resolution. Image resolution can be increased by reducing the field of view (FOV) or increasing the number of samples along a dimension. Decreasing the FOV produces a proportional decrease in the SNR; the FOV must remain larger than the head to avoid excessive ghosting. Increasing the number of samples has less impact on SNR (reduced by square root of the increase[117]). However, increasing the number of samples in the phase encoding direction substantially increases readout time, which increases the amount of T2 decay experienced during slice acquisition and leads to greater in-plane smoothness[118]; parallel imaging mitigates these effects[119].

Considerations for fMRI

BOLD contrast. Spin phase (T2*) contrast is the most sensitive to the BOLD effect and is optimized using an echo time equal to the T2* of gray matter (echo time of ~30 milliseconds at 3 tesla). BOLD can also be measured with spin-echo sequences, which are sensitive to T2 rather than T2* and hence have better spatial specificity, although less sensitivity than gradient echo techniques[120].

Minimizing dropout. Tilting and positioning imaging slices to prevent slices from intersecting air-tissue interfaces can minimize signal dropout resulting from differences in magnetic susceptibility[121]. Slice positioning should focus on areas most vital to the experiment. Reducing echo time, which decreases BOLD contrast, and increasing resolution, which decreases SNR, should be avoided. Specialty sequences (for example, spiral-in/out[122] and z-shim techniques[123]) result in the acquisition of multiple echoes with different dephasing characteristics to reduce susceptibility effects. Alternatively, spin-echo EPI avoids susceptibility artifacts but is much less sensitive to BOLD contrast[120].

Motion sensitivity. Beyond image misalignment, head motion induces fMRI signal fluctuations owing to partial voluming and spin-history effects[39]. Lower flip angles[124], longer repetition time[125] and interleaved slices minimize spin-history effects by allowing the signal in a slice to fully relax before acquisition of the neighboring slice. Spiral sequences are less sensitive to motion during slice acquisition[126]. The 3D imaging techniques minimize the impact of within-volume motion, but between-volume motions remain problematic unless a long repetition time is used; long readouts increase the interaction between magnetic field inhomogeneity and motion[127]. Parallel imaging can improve acquisition time, resolution and bandwidth but requires calibration scans[119]. Misalignments between the acquired data and calibration scans induce reconstruction errors and motion-correlated imaging artifacts[119].

Temporal resolution. Number of slices acquired determines temporal resolution. Echo time fundamentally limits slice-acquisition time. Increasing bandwidth, partial Fourier imaging and parallel imaging can result in marginal speed gains[118].

Considerations for dMRI

Diffusion contrast. Minimizing echo time, and therefore T2 decay, is essential to dMRI. T2 reduces overall magnetic resonance signal and image SNR, and increases in-plane image blurring. Increasing bandwidth, partial Fourier imaging, parallel imaging and using stronger diffusion gradients (b values; high b values require longer diffusion gradient pulses) can minimize echo time[118]. Higher-strength gradient systems enable high b values (desirable for fiber tracking) in shorter

continued

BOX 1 OPTIMIZING fMRI AND dMRI IMAGE ACQUISITION (CONTINUED)

time, though require a hardware upgrade for most systems. Echo shifting also reduces echo time, by relaxing the spin echo condition and shifting the echo train earlier in time[118].

Scan time. Echo time and number of slices determine dMRI volume repetition time. The number of diffusion directions, *b* values and averages acquired determine total scan time.

Emerging acquisition sequences

Multiband and multi-echo imaging are emerging acquisition strategies. In multiband imaging, multiple slices are acquired simultaneously, substantially improving temporal resolution, or increases in spatial resolution per unit time[128], though at the cost of SNR and spatial smoothness. This improvement enables higher fMRI sampling rates and more diffusion directions per *b*-value acquisitions in dMRI[129], substantially improving estimation of macroscale connectomes[130]. In multi-echo fMRI, two echoes of a slice are acquired at each acquisition (one with short echo time and one with an echo time optimized for BOLD imaging[131]). Systematic noise (heartbeat, respiration, head motion and scanner instability) are measured in the first echo (with the short echo time), and removed from the second, enabling signal denoising with practically no SNR cost.

Preprocessing. After acquisition, dMRI data must be preconditioned before directional information can be extracted and tractography can be performed. Little debate exists regarding dMRI data preprocessing (see ref. 14 for an exception), though this may reflect the difficulties of preprocessing and its complex impact rather than consensus in the field.

Correcting image distortions. *In vivo* dMRI data are plagued by spatial distortions, which are a central focus of preprocessing. In particular, magnetic field inhomogeneities are a major contributor. Areas where materials that differ with respect to magnetic susceptibility (that is, extent of magnetization achieved in the MRI) interface with one another (for example, air-tissue interfaces) are particularly prone to such inhomogeneities. These local variations in the magnetic field generate spatial distortions, which can be reduced through parallel imaging techniques or mathematically corrected using estimates of the field variations[15]. Another cause of spatial distortion is the interaction between the static magnetic field and the currents induced by rapid switching of gradients with the magnetic field, known as eddy currents. These artifacts can be reduced using bipolar gradients[16]. Image coregistration, or spatial alignment of brain scans, is commonly used in preprocessing to correct for eddy-current distortions and subject head motion[17]. However, this method is ineffective for images acquired using very strong diffusion gradients. Model-based approaches that explicitly account for the effects of eddy currents during image acquisition are emerging as the preferred option[18].

Overlooked issues. The above preprocessing steps, combined with visual inspection, constitute standard preprocessing. A few important details are often overlooked (see ref. 14 for examples). First, modern scanners are often equipped with antennas that acquire data in parallel through multiple channels that are subsequently combined. Such parallel imaging techniques can increase noise levels if the data are submitted to standard reconstruction[19]. This can artifactually lower diffusivity estimates along the axons, which increases the tendency of tractography approaches to overfit the data and generate false positive connections. An alternative reconstruction method has recently been proposed to address this important issue[19]. Second, any correction of distortion must account

Table 1 | Magnetic resonance imaging parameters

Parameter	Definition	Impact
Echo time	Time between slice excitation and acquiring the center of *k* space	Determines the impact of spin-spin relaxation (T2) and spin dephasing (T2*) on image
Repetition time	The time between acquisitions of adjacent fMRI volumes (sampling period)	Impacts the signal available for imaging (I_0), impacted by the number of slices; longer repetition time durations reduce motion sensitivity
Bandwidth ($1/\Delta_t$)	The range of frequencies mapped to a voxel	Lower bandwidth settings can increase artifacts owing to inadequate shimming or susceptibility and distortions in the phase-encoding direction (for example, 'scalloping')
Flip angle (α)	The amount of rotation applied to proton spins by the excitation pulse	Impacts I_0. Flip angles larger or smaller that the Ernst angle for a given repetition time will reduce I_0. Low flip angles may reduce motion sensitivity and in-flow effects and improve spin-lattice relaxation (T1) contrast of images.
Spatial resolution (Δ_x, Δ_y, Δ_z, N_x, N_y)	The volume of tissue sampled in a given voxel; determined by field of view and the number of points sampled in a slice	Signal-to-noise ratio (SNR) is substantially impacted by voxel volume; higher spatial resolution have lower SNR, for example, a 2-mm isovoxel has only ~30% of the SNR of a 3-mm isovoxel, holding all other factors constant
Parallel imaging (P_f)	Methods such as GRAPPA and SENSE can decrease repetition time and reduce spatial distortions by sampling *k*-space lines in parallel; decreases in repetition time are rate-limited by echo time required for BOLD contrast	Can allow faster image acquisition but at a reduction of SNR by 1/parallelization factor, holding all other factors constant; will increase temporal noise resulting from head motion, respiration or pulsatile effects
N_{acq}	Number of acquisitions that are acquired and subsequently averaged	Improves SNR; does not make sense for fMRI but is commonly used for dMRI

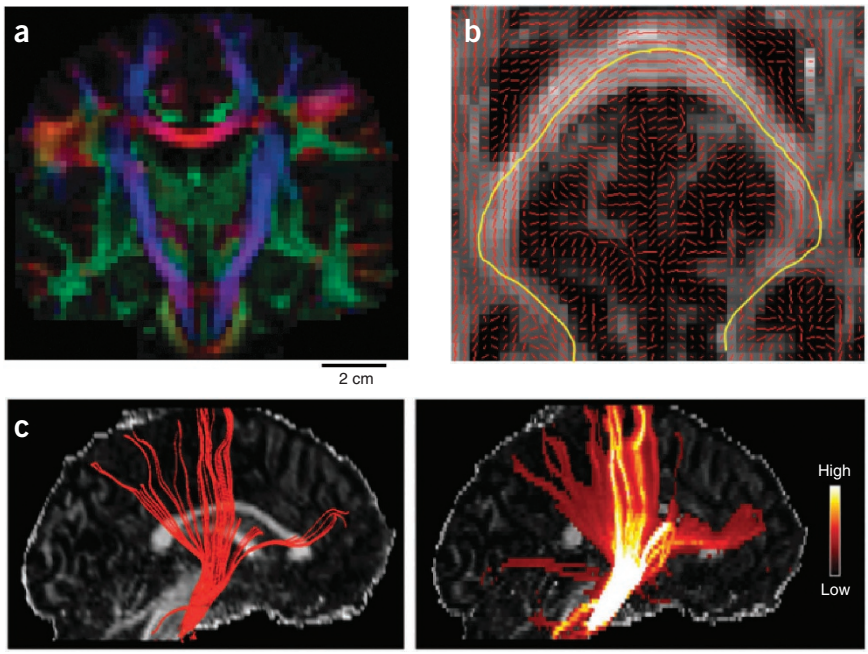

Figure 2 | Diffusion imaging of structural connectivity maps for a human brain. (**a**) dMRI-based map of principal tensor orientations of the human brain viewed from the front. Blue, superior-inferior; green, anterior-posterior; and red, medial-lateral. (**b**) DTI fiber orientation estimates (red lines) from a region of corpus callosum superimposed on a fractional anisotropy image. Sample streamline is in yellow. Image is magnified 4× relative to that in **a**. (**c**) Pyramidal tract streamlines based on deterministic (left) and probabilistic (right) approaches (results superimposed on fractional anisotropy image). Color bar indicates confidence about the presence of the tract. Images courtesy of S. Sotiropoulos (http://etheses.nottingham.ac.uk/1164/).

for voxel-wise compression or expansion during image coregistration. This is particularly important for dMRI, where distortions vary in direction and magnitude between different gradient orientations, but is largely ignored by current software packages. Finally, image coregistrations contain a rotation component that is applied to each volume and must therefore be applied to the concurrent gradient orientation[20].

Estimating fiber orientation. Before delineating tracts and bundles via tractography, fiber orientation(s) must be inferred for white-matter voxels individually. Sensitivity of the dMRI signal to water-diffusion properties (such as rate and direction) enables the estimation of fiber orientation at each voxel. As each voxel contains thousands of axonal fibers, not just one, the goal of dMRI analysis is to infer a probability function for each voxel, which captures the different fiber orientations present and their relative proportions[21]. Estimation of this function— referred to as the fiber orientation density function (fODF)—at each voxel is the first step in estimating structural connectivity.

The diffusion tensor is a simplistic but viable model for the diffusion profile that provides a simple approximation to the fODF[22]. Diffusion tensor imaging (DTI) uses a 3 × 3 matrix to provide an abstract ellipsoid representation of the water-diffusion profile for a given voxel. Mathematical decomposition of this matrix yields information regarding the directions (x, y and z) of maximum and minimum water motion (eigenvectors) as well as the amount of diffusion that occurs along each direction (eigenvalues). The direction of maximal diffusion, referred to as the principal diffusion direction, is taken as the best estimate of fiber orientation within a voxel. Formally speaking, in the case of DTI, the fODF is approximated using a delta function or peak-aligned with the principal diffusion direction.

The diffusion tensor provides a good estimate of fiber orientations when axons are homogeneously aligned within a voxel. However, this is not always the case. Fibers are known to disperse (fan), cross, merge and kiss (temporarily run adjacent to one another)—all of which can happen within a single voxel and lead to heterogeneity not accounted for by a simple delta function. More complex approximations of fODF can account for such heterogeneity within a voxel, though they require greater angular coverage[23,24] (that is, more directions) and models that either explicitly or implicitly account for interactions between fiber orientation and the diffusion signal (see ref. 21 for example methods). Complex fODF models better estimate fiber trajectories, particularly when several white-matter tracts intersect and allow recovery of nondominant pathways invisible to DTI[25].

Estimating edges. After estimation of voxel-wise fiber orientations, tractography approaches are used to establish structural connectivity between connectome nodes. Three-dimensional (3D) trajectories, referred to as 'streamlines', are used to trace putative white-matter paths. Local fiber orientation information guides the construction of streamlines along the fODF, allowing us to trace major white-matter bundles[26]. Results are typically visualized as 3D renderings of thin curves grouped into bundles (**Fig. 2**), reminiscent of postmortem dissection photographs. The individual streamlines do not represent actual axons; they depict estimates of the average trajectories of axon bundles, given our assumption that diffusion is least hindered along axons.

The specific process by which streamlines are developed varies depending on the complexity of the fODF approximations available. With diffusion-tensor modeling, the principal diffusion direction at each voxel guides the formation of the streamline; specifically, it provides a candidate for the tangent to the streamline at each voxel. For more complex fODF models, streamlining follows the same principle, though with multiple peak orientations available at each voxel rather than a single principal diffusion direction. This allows streamlines with differing orientations to pass through the same voxel, which is crucial when heterogeneous fibers are present. Whereas traditional tractography approaches are deterministic, probabilistic approaches account for uncertainty in estimates of local fiber orientations, allowing for estimation of probabilities for any given streamline.

Using streamlining methodologies, it is theoretically possible to measure all connections between gray-matter areas. We can estimate both the trajectories and the end points of anatomical pathways. In practice, however, inference of point-to-point

connectivity using streamlining is imprecise and error-prone[27]; improvements in both data quality and modeling are needed to yield more accurate structural connectomes.

Ideally, we should not only be able to infer the existence or absence of connections between nodes, but estimate connection (edge) strengths as well. Anatomical connections are made up of axons; features of these axons, such as density, size, length and myelination, have important consequences on the propagation of action potentials, and hence information transfer. Measures of microstructural features based on more complex dMRI experiments are emerging[28], and may become an important component of connectomics. Related measures, such as fractional anisotropy and diffusivity, serve as common proxies for these microstructural complexities, but are extremely sensitive to confounding factors such as partial volume (for example, voxels containing a mixture of white matter and gray matter) and axonal dispersion[27,29]. Accordingly, these measures should be used with caution to quantify connection strength. Other anatomical factors such as dendrite densities, spine densities, number of synapses at axon terminals and synaptic efficacy are much harder to determine noninvasively, though potentially are more relevant.

Unfortunately, tractography does not result in quantification of any of the above properties. Often, probabilistic tractography, which provides an estimate in the uncertainty of streamline trajectories, is used to quantify connection strength. Strong connections are expected to have a more discernible trace in the diffusion data and therefore lower uncertainty in their trajectories. This approximation, however, can easily break. For instance, locally nondominant pathways (for example, those that cross larger bundles), have greater uncertainty. Uncertainty is also affected by nonrelevant factors such as signal-to-noise ratio and partial volume effects. Another issue specific to streamlining is that uncertainty in the streamline's path increases with the length of tract. Because streamlining operates by propagating uncertainty spatially, connection probabilities inevitably decrease with distance. As a result, tractography-based structural connections are difficult to quantify, threshold, compare between groups and use for other types of statistical analyses[27,29].

Interpretation and considerations. Pitfalls of tractography can be divided into two categories: accuracy (correctness) and precision (reproducibility)[14]. Accuracy refers to our ability to infer axonal organization from measurements of water diffusion. In the ideal case, there is no instrument-based or physiological noise, yet we can still make erroneous inferences regarding microstructure because of inaccurate modeling. A white-matter voxel contains hundreds of thousands of axons, which do not necessarily align[30]. The fODF models, which account for multiple directions in a voxel (crossing fibers) are replacing tensor models for tractography. However, the subvoxel organization of axons can be more complex than a simple crossing and may not always be easily recovered from the diffusion profile. For instance, a collection of axons that bend in a voxel will create a diffusion pattern that may not be easily distinguishable from that of fiber dispersion. One can easily imagine even more complex situations where all these configurations (for example, bending, dispersion and crossing) happen in the same voxel. Diffusion data from a single voxel cannot be used to unambiguously resolve these complexities. Future approaches may benefit from semiglobal models that aggregate diffusion data across multiple adjacent voxels to infer subvoxel features.

With regard to precision, measurement noise (for example, instrument-based or physiological) and inadequate water-diffusion modeling can compromise tensor and fODF estimation, inducing spurious variations in the generated streamlines. Additionally, use of a fixed step size in the generation of streamlines (despite local variations in anatomy) and the discrete nature of voxels (when tracts are continuous) increase measurement error. Probabilistic tractography algorithms try to quantify these errors by estimating the uncertainty in the entire process. Uncertainty in voxelwise fiber orientation can be quantified[31] and propagated into uncertainties regarding the location of streamlines. This process turns 3D point estimates of streamline trajectories into spatial histograms of their locations (**Fig. 2c**).

Beyond concerns regarding accuracy and precision, identification of fibers in their entirety requires knowledge of where tracts terminate throughout cortex. This remains a challenge for tractography algorithms, which are very good at estimating the location of bundles in deep white matter but not good (yet) at identifying where they project into gray matter[27]. These difficulties result from a lack of detail in white-matter architecture modeled through diffusion and biases in cortical projections.

Estimating functional connectivity

Although the concept of structural connectivity is relatively intuitive given the presence of physical connections between brain areas, its functional counterpart can be more challenging to define. The macroconnectomics field has adopted a neurophysiological perspective of functional connectivity, defining it as the synchronization of neurophysiological events between spatially remote brain areas[32]. First quantified in early electroencephalography and multiunit recording studies, functional connectivity analyses were adopted for positron emission tomography and fMRI in 1993 (ref. 32). Although functional connectivity can be measured noninvasively using a variety of neuroimaging modalities (for example, positron emission tomography, fMRI and magnetoencephalography) and different indices related to physiological function (for example, blood oxygenation level–dependent (BOLD), cerebral blood flow and glucose metabolism analyses), BOLD-based fMRI is the most widely used technique for inferring functional connectivity.

Studies of functional connectivity may be dichotomized on the basis of the presence or absence of a task (that is, T-fMRI versus task-free or 'resting state' fMRI (R-fMRI)). Task-based approaches focus on the detection of synchronous responses to extrinsic stimulation or tasks, referred to here as evoked functional connectivity (eFC) or coactivation[33]. Evoked functional connectivity can be quantified across the entire period of task performance or in response to specific types of events. Approaches using R-fMRI focus on the detection of synchronized spontaneous activity occurring in the absence of experimenter-controlled tasks or stimuli, referred to as intrinsic functional connectivity (iFC)[34]. Although iFC and eFC patterns can be notably similar, especially when eFC is assessed using meta-analytic techniques[35] or broad comparisons (for example, task versus rest), these analyses probe different aspects of the functional architecture[33]. eFC patterns obtained using one task will not necessarily generalize to another, and aspects of iFC obtained during one state may not necessarily

BOX 2 iFC AND CONSCIOUS STATES

The impact of cognitive[97], physiological[132] and pathological states[133] on functional connectivity has been recently demonstrated in the literature. Consciousness has received particular attention, with many studies examining physiological states (for example, sleep), induced states (for example, anesthesia and hypnosis) and pathological states (for example, coma, vegetative syndrome and minimally conscious state[133]). iFC patterns detected in these states are grossly similar to those observed during wakefulness, though direct comparison reveals state-related iFC changes. For example, the default and lateral networks each exhibit decreased functional connectivity among network components (that is, within-network connectivity) during sleep, suggesting decreased integration of information. Complementary findings of decreased negative iFC between these networks and others may suggest decreased segregation as well[134]. These results suggest that although sleep-based studies may be useful in populations not amenable to examination in wakeful states (for example, toddlers), comparison of findings across states may be problematic. Of note, changes in thalamocortical connectivity are reported during anesthesia, non–rapid eye movement (non-REM) sleep and vegetative states[135], but the specific role of thalamocortical circuitry in consciousness remains underexplored. These studies also suggest potential clinical applications of iFC, such as improving recognition of consciousness after recovery from coma.

generalize to another (for example, wakefulness and sleep; see **Box 2** for a discussion of states other than wakeful rest).

Acquisition. BOLD is the predominant fMRI technique used in studies of functional connectivity (see ref. 36 for alternative cerebral blood flow–based technique). BOLD is measured using ultrafast imaging sequences that are sensitive to relative concentrations of deoxyhemoglobin, which is paramagnetic (that is, dephases the magnetic resonance signal), in contrast to oxyhemoglobin, which is diamagnetic[37]; the resulting measurement is an indirect measure of neural activation. Data sets for functional-connectivity analysis using fMRI are typically obtained in 5–30 minutes, as a participant either performs an experimental task (T-fMRI) or rests quietly in the scanner (typically while awake; R-fMRI). We discuss determinants of BOLD imaging acquisition quality in **Box 1**.

Preprocessing. The aim of preprocessing is to remove confounding variation from data and facilitate comparison across subjects. Structured nuisance signals and anatomical variation can obscure functional connectivity measurements if left unaccounted for. Despite considerable effort, we lack consensus regarding the optimal set of preprocessing steps, their ordering and their implementation. Most preprocessing steps originated with task-activation approaches. However, their use and implications are greater for functional-connectivity approaches because of the greater risk of spurious findings given that the independent and dependent variables can be contaminated by the same noise signals (for example, motion and respiration). Comprehensive comparison of preprocessing strategies and their implications for eFC and iFC analyses remain elusive, in part owing to a lack of objective benchmarks. The preprocessing steps described below are post-*hoc* corrections. However, optimization of acquisition strategies to minimize the impact of noise sources is preferred (**Box 1**).

Slice timing correction. The slices of an fMRI volume are acquired at different times, creating effective shifts in time series obtained at different slices. Although some question its necessity[38], correction by temporal interpolation is recommended to avoid the potential for deleterious impact of these lags on signal denoising and time-series extraction from brain areas.

Motion correction. Head motion results in a misalignment of brain areas between volumes typically accounted for using 3D image-registration techniques. Additionally, head motion induces artifactual fMRI signal fluctuations resulting from changes in slice tissue composition (partial voluming) and residual magnetization from prior slice excitations (spin-history effects)[39]. These motion artifacts are typically modeled and removed in a regression framework, containing predictors calculated from motion parameters estimated during coregistration[40]. Although effective, modeling-based approaches do not completely remove motion-related fluctuations in the fMRI signal[41–43]. To address this issue, the 'scrubbing' of offending volumes via removal[41] or spike regression[44] has been proposed. Excluding time points alters the temporal structure of the data, thereby compromising analyses that rely on this structure (for example, temporal dynamics, spectral analysis and estimation of temporal autocorrelation). Regardless of the motion-correction scheme used, it is necessary to account for motion in group-level analyses[42,45].

Physiological noise correction. Cardiac pulsation and respiration can induce fMRI signal fluctuations, which had led to early criticisms attributing iFC to these physiological signals rather than neural signals[46]. The cardiac cycle generates pulsatile motion throughout the brain[47]. Respiratory movement of the chest and abdomen induce changes in the magnetic field, producing intensity fluctuations in fMRI images[47]. Additionally, changes in cardiac rhythm as well as rate and depth of breathing create longer-term effects. Respiration and pulse can be recorded to model and subsequently remove their impact[47]. Although this is accepted as ideal, it is not commonly performed. Instead, signals present in white matter and cerebrospinal fluid are taken as surrogates for respiration and cardiac effects, and regressed from the fMRI time series. Incorporating spatial variation in the noise captured by the white-matter signal provides superior denoising (for example, anatomy-based correlation corrections (ANATICOR)[48]). Blinded source-separation techniques provide another means of physiological correction (for example, Corsica[49]).

Global signal regression. The mean time series across the whole brain is commonly regressed from the data. In this model, the global signal is considered a nonspecific measure of noise, whose removal improves the specificity of iFC[50], decreases motion effects[44], and

removes intersession and intersite effects. However, awareness that global signal regression centers the correlation distribution at zero, and thus introduces negative connections[51] and can alter inter-individual differences[52], has made its use controversial. In this regard, it is important to note that functional correlation coefficients obtained after global signal regression are relative values, not absolute. Additionally, electrophysiological demonstrations of globally synchronous neural signals in gray matter[53] call into question the interpretation of the global signal as simply noise.

Temporal filtering. Bandpass filtering is usually performed to remove frequencies below 0.001 hertz and greater than 0.08 hertz from the fMRI time series. This frequency range targets removal of low-frequency scanner drift and frequencies above those traditionally associated with functional connectivity[34,54]. However, complete removal of physiological noise is unlikely because of artifacts induced by the low-temporal-resolution of fMRI (for example, aliasing)[46]. Concerns about temporal filtering include reductions in the degrees of freedom for the time series and recent demonstrations of functional connectivity at frequencies greater than 0.1 hertz for several brain areas, suggesting that low-pass filtering is removing valuable signal[55]. Thus, despite historical precedent, inclusion of low-pass filtering merits additional consideration.

Spatial normalization and smoothing. Another aspect of preprocessing is conditioning the data for comparison across subjects. Spatial normalization addresses morphological variation across individuals by transforming subject data to a common stereotactic space; population- and study-specific templates are increasingly used to optimize correspondence. Spatial smoothing additionally improves the correspondence of brain areas across individuals and increases the signal-to-noise ratio[56].

Estimating edges. Several mathematical modeling techniques can be used to define functional relationships, differing primarily in the stringency with which they define functional connectivity. Functional connectivity simply implies a statistical dependency between activities observed in brain areas and is an umbrella term for a wide range of dependency measures, each providing a different perspective[32]. For example, mutual information measures statistical dependency from the joint-probability distribution function and is sensitive to linear and nonlinear relationships, whereas Pearson's correlation is primarily sensitive to linear relationships[57]. Effective connectivity, in contrast, requires a mathematically precise (directional) description of the interactions between brain areas[58]. This leads to a plurality of graphs that can be derived from functional connectivity, with each graph characterizing functional interactions from a different perspective.

Estimating iFC from R-fMRI data typically begins with extraction of the mean time series across voxels in each brain node (that is, parcellation-defined brain area). Intrinsic functional connectivity is commonly estimated from bivariate tests for statistical dependency (for example, Pearson's correlation, mutual information and spectral coherence) between every possible pairing of time series[59]. Although these approaches perform well in simple simulations[59], the limited number of observations results in noisy estimates of statistical relationships, which can be reduced using regularization (shrinkage) methods[60]. A limitation of bivariate approaches is that they do not account for information from multiple brain areas simultaneously. Hence they cannot be used to distinguish direct from indirect interactions (mediated by common relationships with other areas). Partial correlation (related to the inverse covariance matrix) results in estimates of the conditional linear dependency between two brain areas, after accounting for interactions with every other area[61]. Although this approach is preferred to bivariate approaches, the number of brain areas commonly exceeds the degrees of freedom, preventing unique specification of partial correlations. In these cases, regularization techniques (for example, graphical lasso and elastic net) can be used to find a solution[59]. Additionally, information can be pooled across individuals to optimize estimation parameters[62]. Note that some, but not all, of these approaches enforce symmetry; in other words, one can obtain dependency in one direction but not the other (**Box 3**).

Many approaches exist for estimating eFC. Several authors have borrowed approaches used to examine iFC; such approaches are based on the assumption that the time series spans the entire task[63] or concatenated blocks of specific task conditions[64]. Psychophysiological interaction[39] analyses directly model interactions between patterns of functional connectivity and the experimental stimulus design, potentially offering greater specificity of findings. Others have measured eFC from 'coactivation' using fitted regression coefficients[65] or binarized (by applying a threshold to regression coefficients) time series[66] generated from a first-level task analysis. Regression coefficient series are then compared using correlation or partial correlation[33,65]. Binarized time series can be compared from the joint distribution of the two values using measures akin to mutual information[66]. Finally, meta-analytical approaches provide a means of measuring eFC across studies and often tasks, enabling detection of patterns of coactivation across statistical maps generated from data in the literature[35,67].

A variety of data-driven techniques are also used for identifying iFC and eFC patterns. Examples include self-organizing maps[68], principal component analysis, normalized cut clustering[69] and independent component analysis[70]. These methods are more appropriate for identifying nodes of connectome graphs than edges, although exceptions exist[59].

Once functional connectivity is estimated, some applications require it to be thresholded or binarized (that is, to determine whether a connection is present or not). Threshold selection is not straightforward but can be accomplished by applying a test of statistical significance to each edge. When using parametric statistics, care must be taken to adjust the degrees of freedom for temporal autocorrelation. Alternatively, this can be addressed using nonparametric tests of significance such as wavestrapping[71] or circular-block bootstrap[72]. Sparse covariance estimation methods can also be used.

Interpretations and considerations. A common pursuit of T-fMRI and R-fMRI studies is to fractionate the connectome into a set of spatially and functionally distinct networks that can each be annotated in terms of the specific functionality domain they subserve (for example, cognitive, affective or visceral). It is impressive that these T-fMRI and R-fMRI studies have converged on similar definitions of 8–20 spatially and functionally distinct networks, though studies have suggested the actual number of networks is substantially greater[13]. The concordance of T-fMRI and R-fMRI findings suggests the brain's intrinsic functional architecture

BOX 3 DIRECTIONALITY IN FUNCTIONAL CONNECTOMICS

Commonly referred to as effective connectivity, the mapping of directional relationships is essential for characterizing information flow in functional-connectivity studies[136]. Identification of neural drivers can facilitate our understanding of control systems as well as ectopic foci leading to pathological conditions (for example, epilepsy[137]). Although invasive tracing and stimulation techniques are powerful tools for mapping directional relationships in nonhuman populations[138], they are not generally applicable in humans. Here we provide an overview of noninvasive approaches to establishing directionality.

Statistical techniques

Before reviewing statistical effective connectivity approaches, we note that despite the nomenclature, their findings should not be interpreted as indicating causality but rather the directionality of information flow. Structural equation modeling (SEM) and dynamic causal modeling (DCM) approaches evaluate the fit of hypothesized models of directional interactions among nodes with measured fMRI data. SEM is a covariance-based approach that represents each node as an exogenous variable (predicting the activity of another node), endogenous variable (activity is predicted by another node) or both[139]; effective connectivity is modeled at the hemodynamic (BOLD response) level. In contrast, DCM is a generative approach, modeling effective connectivity at the neuronal level based on a given biophysical model and uses a forward model to produce the downstream fMRI activity. Models can be evaluated individually; however, common practice is to compare models representing competing hypotheses regarding causality to identify the 'best-fit' model. Concerns exist regarding the feasibility of successfully identifying a 'best fit' model from a large population of putative models[140]. SEM and DCM approaches are limited in the number of nodes and interactions they can model efficiently. Primarily intended for confirmatory analysis, exploratory implementations of SEM[141] and DCM[136] are emerging for use with R-fMRI.

Granger causality analysis (GCA) is a model-free, data-driven effective connectivity approach[142] that investigates whether past values of the time series for one node could improve the prediction of the current value in another[143]. In contrast to SEM and DCM, GCA can be used to assess many nodes simultaneously. Application of GCA to R-fMRI[144] is particularly controversial because of (i) limitations imposed by the sluggish and variable hemodynamic response function (HRF), (ii) slow sampling rate (for example, repetition time ≥2 s)[59] and (iii) assumptions that HRF characteristics are constant across nodes[59]. Attempts to rehabilitate GCA for R-fMRI include HRF deconvolution before GCA[137], accounting for regional variation in the HRF using breath-hold scans and faster sampling rates[145]. Nonetheless, using GCA with R-fMRI remains problematic.

Lesion studies

Lesion studies directly perturb the system and therefore can be compelling in establishing causality when carried out in a controlled manner. From this perspective, changes in the activity of a node after disruption of inputs from another are taken to infer causal influences. In the ideal paradigm, scans are obtained before and after occurrence of a given lesion. For example[146], R-fMRI scans from the brain of a 6-year-old child before and after callosotomy revealed disruptions specific to interhemispheric connectivity. Lesion studies are, however, commonly limited to scans after lesion, taken after natural occurrence of lesions (for example, stroke, congenital abnormality, neoplasm and seizure focus). Although useful for testing predictions or generating hypotheses, findings of such studies cannot be considered definitive.

Brain stimulation

The gold standard for establishing directional influences is the demonstration that direct stimulation of node A impacts node B but not the converse. In this regard, intraoperative studies of corticocortically evoked potentials—which involve the tracking of electrical signals from stimulation sites to other locations—are powerful tools[147], though with limited applicability (that is, in neurosurgical patients). Noninvasive stimulation techniques with a broader range of applications are slowly evolving. Transcranial magnetic stimulation (TMS) can be used to produce temporary and reversible neural excitation or suppression in targeted cortical areas. Concurrent TMS-fMRI studies have revealed causal relationships in motor circuits[148] and the visual system[149]. Transcranial direct-current stimulation and transcranial alternating-current stimulation approaches deliver weak currents to targeted brain areas, and are emerging as less expensive and technically demanding alternatives to TMS, though delivering focal stimulation is challenging[150].

provides a framework for moment-to-moment responses to the external world. As summarized in ref. 67, it appears that "the full repertoire of functional networks utilized by the brain in action is continuously and dynamically 'active' even when at 'rest'."

When considering the visualization of functional connectivity (**Fig. 3**), an important question is: 'what are we missing?'. Whereas functional connectivity is often represented with static graphs, neurophysiological models have long asserted the transient nature of many functional interactions. Specifically, distributed neural assemblies appear to change their patterns of interaction with one another from one cognitive act or state to another. Consistent with this notion, eFC studies have noted substantial task-dependency in their findings, even when looking at the same regions[33,39]. Perhaps most exciting, recent iFC studies have observed dynamic changes in iFC patterns over a 5-minute scan[73]. These findings suggest that commonly used metrics of iFC are incomplete, only capturing the 'mean' connectivity over time. If true, the implications would be multifold: (i) findings of hypo- or hyper-connectivity in population studies would need to be reassessed, as they may reflect a different distribution of time spent in the various iFC configurations between populations, and (ii) the detection of changing eFC patterns over the course of task performance may prove to be a means of explaining observed behavioral variability. More and

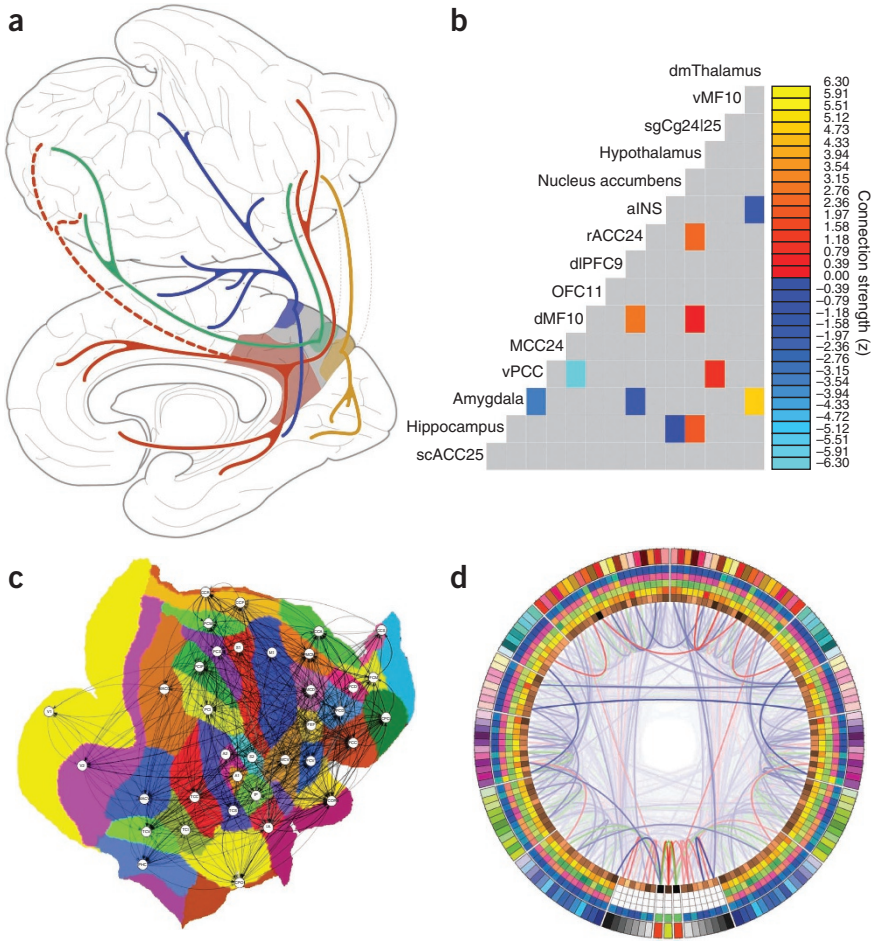

Figure 3 | Visualizing the connectome. (**a**) Classical anatomical-tracing–style depiction of iFC for posteromedial cortex subdivisions (image reproduced from ref. 113). (**b**) Matrix representation of functional brain connections predictive of diagnostic status in depression. dmThalamus, dorsomedial thalamus; vMF10, ventral medial prefrontal cortex (Brodmann area (BA) 10); sgCg24|25, subgenual cingulate (BA 24 and 25); aINS, anterior insula; rACC24, right anterior cingulate cortex (BA 24); dlPFC9, dorsolateral prefrontal cortex (BA 9); OFC11, orbitofrontal cortex (BA 11); dMF10, dorsal medial prefrontal cortex (BA 10); MCC24, midcingulate cortex (BA 24); vPCC, ventral posterior cingulate cortex; scACC25, subcallosal cingulate cortex (BA 25) (image reproduced from ref. 90). (**c**) Flatmap-based representation of the CoCoMac atlas of the macaque connectome (image reproduced from ref. 114). (**d**) Connectogram depicts brain areas (nodes) as columns in the circular band, differing connectivity metrics in separate layers and connections with lines; lobes are differentiated by color, and left or right halves corresponds to hemispheres (reproduced with permission from ref. 115).

more studies are highlighting the potential value of examining transition zones between functional areas in the brain[5]. Examination of temporal dynamics may inform such efforts, by mapping changes in the boundary over time and providing greater clarity for findings.

In addition to naturally occurring variations in iFC over time, studies have suggested that iFC can be systematically impacted by cognitive demands before R-fMRI data acquisition. By comparing iFC during R-fMRI scans collected before and after task performance[74], studies show that iFC strength within and between networks is altered in a task-dependent manner. For example, R-fMRI–based functional connectivity between the inferior frontal gyrus and visual areas varied depending on the category of stimuli viewed before the R-fMRI scan[75]. Across participants, the extent to which iFC was modulated correlated with subsequent memory for the stimuli. In addition to exhibiting plasticity related to tasks performed close in time to the measurements, iFC is modulated by direct-stimulation protocols including median nerve stimulation[76], heat pain[77], transcranial magnetic stimulation[78] and transcranial direct current stimulation[79]. This suggests that R-fMRI may have utility in the identification of targets for stimulation protocols as well as assessment of their efficacy (for example, in the context of the treatment of depression[80]).

This iFC-based evidence of experience-induced plasticity provides strong support for the hypothesis that iFC reflects a history of coactivation among areas. However, this also suggests a corollary: correlated intrinsic activity has a role in learning and memory consolidation[81]. The demonstration of brain-behavior correlations between task-related modulations of iFC and subsequent behavior (for example, recall) supports this hypothesis. If short-term iFC alterations reflect experience-induced plasticity, then enduring changes would be expected after extended practice or training. Several studies suggest this is the case[82]. Studies of long-term training–induced plasticity have the potential to inform our understanding of mechanisms involved in remediation-based recovery of function or even to index the efficacy of treatment interventions. For example, in a preliminary retrospective study, differences in iFC were observed between children with dyslexia who were remediated by reading interventions versus children who received no treatment[83].

Statistical analysis of the connectome

Once connectome graphs are estimated, the next goal is to annotate them in terms of their relevance to higher-order cognitive processes, neuropsychiatric diagnoses or other phenotypic variables[5]. These associations are most often inferred by performing a categorical or dimensional statistical analysis that compares connectivity across a population of individuals or within an individual across time or treatments[84]. Many of the same statistical approaches are appropriate for the analysis of connectome graphs regardless of whether they were constructed with functional or structural data sets. However, the interpretation of the results must always account for the idiosyncratic differences between structural and functional connectivity. For example, functional connections are typically weighted and can be positive or negative. Structural connectivity graphs tend to be unweighted and are strictly nonnegative[27]. Additionally, structural connections can be thought of as pathways along

which information can flow, but functional connections cannot be interpreted in the same manner[85].

A bag of edges. The simplest approach to compare graphs is to treat them as a bag, or collection, of edges and perform statistical analyses at each edge one at a time, without taking into account interactions or relationships between them (that is, edgewise statistics)[84]. Such univariate approaches (for example, *t*-tests, *F*-tests or regression) allow researchers to identify easily interpretable relationships between categorical or dimensional variables and edge weights. However, this approach results in the need to perform many statistical tests, which require correction for multiple comparisons to adequately control for the number of false positives. Standard correction techniques such as false discovery rate[86] that do not model the dependencies between edges may result in overly liberal or conservative corrections[87]. Alternate correction techniques such as the network-based statistic[88] or group Benjamini-Hochberg[89] leverage information about the group structure of connectome graphs to increase statistical power, while maintaining control of false positives.

Alternatively, multivariate regression and classification techniques evaluate the relationship between the entire connectome graphs and their associated phenotypic variables with a single statistical test[90,91]. Although powerful for the analysis of connectome-phenotype relationships, they obscure information about the involvement of individual edges. Extracting this information, if desired, requires a return to edge-specific tests, and the need for multiple-comparison correction[90]. Although these multivariate techniques tend to be applied to bag-of-edges representations, which ignore graph structure, they can also be performed using graph-distance measures that preserve topological information when comparing graphs[92].

Node and graph-level statistics: invariants. Graphical representations of connectomes contain a wealth of information about brain architecture beyond the presence and strength of bivariate connections, which can be described using a variety of node-level and graph-level statistics. These measures are called 'invariants' in graph-theory parlance or 'topological measures' in network-theory parlance because they are not unique to particular representations of the graph. The most commonly used node invariants are centrality measures that indicate a node's relative influence in a graph. Several different centrality metrics are available that measure a node's importance on the basis of the number and strength of direct connections (degree centrality[93]), the importance of neighboring nodes (eigenvector[94] or Page Rank[95] centrality) and their role in connecting other pairs of nodes (betweenness[85]). The various measures provide different perspectives on a node's role in the graph and, when combined, can lead to a more holistic understanding of connectome-phenotype relationships[95].

Similarly, a range of graph-level invariants is used for studying structural and functional connectivity. In particular, graphs are commonly assessed in terms of their local and global efficiency. Local efficiency assesses the extent to which neighbors are densely interconnected, whereas global efficiency captures the number of connections that must be traversed to connect any two nodes[93]. The relationships of these two measures to what would be obtained from random graphs with similar properties can be combined to assess the 'small-worldness' of a graph[93]. Small-world graphs balance integration and segregation to obtain fast and cost-efficient propagation of information through the graph as well as robustness to single-node failures[96]. The cost-efficiency of a graph can be inferred from the difference between global efficiency and the number of edges in the graph[93]. An additional invariant is modularity, which quantifies the extent to which a graph can be segregated into densely intraconnected but sparsely interconnected modules and allows direct comparison of module membership between graphs[85].

Each of the previously described node and graph invariants can be statistically evaluated to identify relationships with categorical and dimensional phenotypes. Although invariants can increase statistical power by decreasing the number of multiple comparisons, the resulting relationships can be more difficult to interpret. When comparing invariants between graphs, it is important to consider the impact of potential differences in graph properties (for example, number of edges) that can systematically differ between individuals or groups and confound interpretation of findings[93]. Additionally, as the distribution properties of most invariants are poorly characterized, nonparametric statistical tests are preferred[93].

Predictive modeling

Finally, researchers frequently aim to identify connectivity patterns predictive of a phenotypic variable (for example, diagnosis[90], age[91] or brain state[97]). Predictive modeling can be used to directly assess the ability of a connectivity pattern to predict the phenotype of an individual, in contrast to inferential statistics, which evaluate improbability of a set of relationships arising by chance[98]. Predictive modeling is typically supervised, with the training set consisting of connectivity graphs and their associated phenotypes[99]. One can assess the predictive accuracy via cross-validation[99] or other model-selection techniques. Predictive modeling has primarily focused on invariants and bag-of-edges–style[90,100] approaches.

Translational connectomics

MRI-based approaches to connectomics research are rapidly transforming neuroscience in animal models as well, by removing barriers to longitudinal examinations associated with invasive techniques (for example, animal killing and injection of toxic chemicals). The recent Mouse Biomedical Informatics Research Network initiative (http://www.loni.ucla.edu/BIRN/Projects/Mouse/) provides an initial demonstration of the potential to complement cross-sectional atlases of the developing brain generated using histology approaches with longitudinal atlases obtained using dMRI. Simultaneously, R-fMRI is emerging as a powerful tool for comparative functional neuroanatomy studies. Initial work has demonstrated impressive correspondence between the iFC observed in humans and macaques for homologous functional networks supporting an array of functions, including those that are putatively 'human' (for example, language, self-referential processes and cognition)[101]. Evidence of homologies with patterns of iFC in lower mammals, such as rats, underscores this translational potential[102]. Armed with increasingly powerful imaging-based tools, macroscale connectomics studies in animal models are poised to provide a mechanistic understanding of brain function through the combination of noninvasive imaging with direct structural, pharmacological, molecular and genetic manipulations that are impossible in humans.

Table 2 | Initiatives promising to accelerate macroscale connectomics research

Initiative (weblink when available; location)	Goals
Brain Genomics Superstruct (United States)	Aims to collect a large-scale imaging data set to explore brain–behavior relationships and their genetic influences. The initiative has collected R-fMRI, dMRI and saliva samples from over 3,000 adults, along with comprehensive phenotyping data (cognition, personality and lifestyle), and the resultant repository containing 1,500 completed, quality-pass data sets is expected to be publicly available in 2013.
Brainnetome (http://www.brainnetome.org/; China)	Attempts to characterize brain networks with multimodal neuroimaging techniques, from the microscale (microtechnique, ultramicrotomy, staining and visualization techniques) to the macroscale (electroencephalography, fMRI and dMRI). R-fMRI and diffusion-imaging data sets, along with behavioral and blood data from more than 1,000 patients with schizophrenia, 300 patients with Alzheimer's disease and mild cognitive impairment, 120 patients who had a stroke, 50 patients with glioma and 2,000 healthy controls collected from 11 hospitals and imaging centers.
Consortium of Neuroimagers for the Noninvasive Exploration of Brain Connectivity and Tracts (http://www.brain-connect.eu/; European Union)	Consortium focused on studying the brain's microstructure, tracts and connectivity using dMRI. Target deliverables include optimized acquisition protocols, analytic tools and a connectivity atlas.
Developing Human Connectome Project (European Union)	Initiative to comprehensively map and model the human connectome for 1,000 babies, including *in utero* and *in vivo* imaging (20–44 weeks after conception).
US National Institutes of Health Human Connectome Project: Washington University in Saint Louis–University of Minnesota consortium (http://humanconnectome.org/; United States)	State-of-the-art multimodal imaging initiative (R-fMRI, T-fMRI, dMRI and magnetoencephalography) that makes use of a twin design (1,200 healthy adults, including twin pairs and their siblings from 300 families) to provide insights into relationships between brain connectivity, behavior and genetics. The project uses multiband imaging sequences for R-fMRI (high spatial and temporal resolution) and dMRI (high spatial resolution), which it has refined and is currently distributing to interested centers. All data and tools developed through the initiative will be openly shared.
US National Institutes of Health Human Connectome Project: MGH-Harvard-UCLA consortium (http://humanconnectomeproject.org/; United States)	Initiative focusing on unraveling the full connectivity map using the first 'Connectome Scanner', which is designed to carry out diffusion using ultrahigh gradient strength (4–8 times the strength of conventional systems). Efforts to optimize dMRI technology will focus on increasing the spatial resolution, quality and speed of acquisition.
1000 Functional Connectomes Project (FCP) (http://fcon_1000.projects.nitrc.org/; global)	Grass-roots data-sharing initiative that brought together over 1,200 previously collected R-fMRI data sets from 33 independent sites around the world and released them openly to the scientific community via the Neuroimaging Informatics Tool Resources Clearinghouse (http://www.nitrc.org/).
International Neuroimaging Data-sharing Initiative (INDI) (global)	Second FCP initiative that was founded in an attempt to (i) expand the scope of open data sharing in the functional neuroimaging community to include phenotypic data beyond age and sex (major INDI data releases: ADHD-200 Consortium (http://fcon_1000.projects.nitrc.org/indi/adhd200/), the Autism Brain Imaging Data Exchange (ABIDE; http://con_1000.projects.nitrc.org/indi/abide/)) and (ii) provide a model for prospective, prepublication data sharing (major release: the Nathan Kline Institute-Rockland Sample http://fcon_1000.projects.nitrc.org/indi/enhanced/). More than 5,000 R-fMRI data sets are available through the FCP and INDI efforts combined as well as a growing number of dMRI data sets.
UK Biobank Imaging (http://www.ukbiobank.ac.uk/; UK)	Building on an existing long-term prospective epidemiological study that has collected genetics, blood samples and lifestyle information from a cohort of 500,000 subjects, the UK Biobank Imaging Extension aims to resample 100,000 of the cohort using multimodal neuroimaging (including but not limited to R-fMRI and dMRI), as well as cardiac MRI and rich phenotyping.

Large-scale initiatives from around the world that are promising to accelerate the pace of macroscale connectomics research through either the advancement of macroconnectomics research through the generation and sharing of large-scale imaging data sets with phenotyping or innovation of data-acquisition and/or analysis techniques (see ref. 116 for additional information regarding these initiatives and others).

Despite the rich promise of translational connectomics, methodological issues must also be addressed. For example, iFC can be examined in awake rats that have been habituated to restraint in the loud MRI environment[103]. However, most studies are conducted under anesthesia—in particular, using the general anesthetic isoflurane[104], which can confound findings owing to its effects on neural excitability. The sedating alpha-2 adrenergic agonist medetomidine may be preferable as it avoids such confounds[105]. Dose-response studies of anesthesia are few[104] and are essential. Initial translational studies in monkeys, rats and mice have relied on preprocessing and analytical approaches identical to those developed in humans[103]. Although their success is encouraging, differences in physiological (for example, cardiac activity and respiration) and imaging parameters must be explored to arrive at optimal strategies. Finally, we note that the many questions raised regarding the interpretation of dMRI and R-fMRI techniques in humans also apply to animal studies.

Toward neurophenotypes and clinical applications

An overarching goal of the connectomics era is the derivation of 'neurophenotypes'[106], a concept that remains poorly specified despite increasing enthusiasm from investigators. An individual's macroscale connectome and its subgraphs contribute to the specification of that individual's neurophenotype. A central goal of connectomics is to catalog neurophenotypes and relate them to phenotypic profiles[4]. This can be accomplished through data-driven approaches focused on the detection of commonalities and distinctions in connectomes or by differentiating populations of neurophenotypes based on their phenotypic profiles. The breadth of phenotyping can vary depending on the application, though it typically consists of some combination of cognitive, affective, behavioral, neurological or psychiatric variables. When cataloging neurophenotypes based upon macroscale connectomes, the specificity of findings will depend on their nature, granularity of node definitions and quality of neuroimaging data used. Similarly,

Table 3 | Connectomics studies in clinical populations

Neuropsychiatric diagnoses	R-fMRI count	dMRI count
Schizophrenia	100	283
Alzheimer's disease	89	201
Depression	81	101
Epilepsy and seizures	62	179
Mild cognitive impairment	58	115
Other neurological disorders	45	50
Substance dependence	40	94
Attention deficit hyperactivity disorder	32	37
Autism spectrum disorders	26	86
Multiple sclerosis	22	211
Parkinson's disease	19	73
Traumatic brain injury	18	259
Sleep disorders	17	7
Stroke	15	182
Anxiety disorders	15	16
Coma and vegetative state	15	9
Obsessive compulsive disorder	12	27
Amyotrophic lateral sclerosis	10	84
Bipolar disorder	10	61

Neuropsychiatric disorders most commonly studied using macroscale functional and structural connectivity. Determined by the number (count) of R-fMRI and dMRI papers dedicated to the neuropsychiatric diagnosis. Calculated from the Child Mind Institute Librarian (Resting State and DTI libraries; (http://www.mendeley.com/profiles/cmi-librarian/).

when sorting neurophenotypes on the basis of phenotypic profiles, specificity will be determined by the precision and comprehensiveness (that is, number and breadth of independent features) of the phenotyping available to statistical analysis. Future work will need to find a balance between categorical and dimensional perspectives of neurophenotypes.

Beyond the derivation of a fundamental understanding of brain architecture and its implications for behavior and cognition, a major reason for the excitement surrounding connectomics is the promise of clinical utility because of the ability to obtain individual-relevant reliable brain indices (see **Table 2** for initiatives that are accelerating the pace of macroconnectomics research). Recent years have witnessed an explosion in the number of neurological and psychiatric disorders studied with dMRI and R-fMRI (**Table 3**). Hopes of attaining clinically useful diagnostic tools are increasingly espoused in the literature. However, leaders in the field have recently suggested that the attainment of tools capable of stratifying individuals based upon disease risk, prognosis and treatment response may prove to be a more fruitful goal than focusing on diagnosis[107]. Regardless, a key requirement remains: attaining large-scale data sets representative of the human population. In this regard, the macroconnectomics community has supported several large-scale data-sharing initiatives dedicated to rapidly aggregating the necessary data[108].

Conclusion

The connectomics era is the culmination of more than a century of conceptual and methodological innovation. MRI-based approaches to mapping and annotating the connectome at the macroscale are transforming basic, translational and clinical neuroscience research by overcoming barriers to progress faced by more traditional invasive methodologies. In this Review we broadly surveyed the many challenges that remain in the acquisition, preprocessing and analysis of brain-imaging data. Failure to consider the many complexities could jeopardize this burgeoning field through the introduction of spurious, irreproducible findings associated with suboptimal methodologies. Conversely, increased attention to the acquisition of high-quality data, combined with optimized preprocessing and analytic methodologies can serve to accelerate the pace at which connectomes can be meaningfully annotated and their variations cataloged.

ACKNOWLEDGMENTS

This work was supported by grants from US National Institute of Mental Health (BRAINS R01MH094639 to M.P.M. and K23MH087770 to A.D.M.), the Stavros Niarchos Foundation (M.P.M.), the Brain and Behavior Research Foundation (R.C.C.) and the Leon Levy Foundation (C.K. and A.D.M.). J.T.V. receives funding from the London Institute for Mathematical Sciences HDTRA1-11-1-0048 and US National Institutes of Health R01ES017436. Additional support was provided by a gift from Joseph P. Healey to the Child Mind Institute (M.P.M.). We thank D. Lurie for his assistance in the preparation of the manuscript and references as well as Z. Shehzad, Z. Yang and S. Urchs for their helpful comments. We acknowledge our colleagues who allowed us to reproduce their figures.

COMPETING FINANCIAL INTERESTS

The authors declare competing financial interests: details are available in the online version of the paper.

1. Sporns, O., Tononi, G. & Kötter, R. The human connectome: A structural description of the human brain. *PLoS Comput. Biol.* **1**, e42 (2005).
2. Varela, F., Lachaux, J.P., Rodriguez, E. & Martinerie, J. The brainweb: phase synchronization and large-scale integration. *Nat. Rev. Neurosci.* **2**, 229–239 (2001).
3. Biswal, B.B. *et al.* Toward discovery science of human brain function. *Proc. Natl. Acad. Sci. USA* **107**, 4734–4739 (2010).
4. Behrens, T.E.J. & Sporns, O. Human connectomics. *Curr. Opin. Neurobiol.* **22**, 144–153 (2012).
5. Kelly, C., Biswal, B.B., Craddock, R.C., Castellanos, X.F. & Milham, M.P. Characterizing variation in the functional connectome: promise and pitfalls. *Trends Cogn. Sci.* **16**, 181–188 (2012).
6. Talairach, J. & Tournoux, P. *Co-planar Stereotaxic Atlas of the Human Brain* (Thieme Classics, 1988).
7. Margulies, D.S. *et al.* Mapping the functional connectivity of anterior cingulate cortex. *Neuroimage* **37**, 579–588 (2007).
8. Beckmann, M., Johansen-Berg, H. & Rushworth, M.F.S. Connectivity-based parcellation of human cingulate cortex and its relation to functional specialization. *J. Neurosci.* **29**, 1175–1190 (2009).
9. Dosenbach, N.U. *et al.* A core system for the implementation of task sets. *Neuron* **50**, 799–812 (2006).
10. Bellec, P. *et al.* Identification of large-scale networks in the brain using fMRI. *Neuroimage* **29**, 1231–1243 (2006).
11. Craddock, R.C., James, G.A., Holtzheimer, P.E., Hu, X.P. & Mayberg, H.S. A whole brain fMRI atlas generated via spatially constrained spectral clustering. *Hum. Brain Mapp.* **33**, 1914–1928 (2012).
12. Cohen, A.L. *et al.* Defining functional areas in individual human brains using resting functional connectivity MRI. *Neuroimage* **41**, 45–57 (2008).
13. Kiviniemi, V. *et al.* Functional segmentation of the brain cortex using high model order group PICA. *Hum. Brain Mapp.* **30**, 3865–3886 (2009).
14. Jones, D.K. Challenges and limitations of quantifying brain connectivity *in vivo* with diffusion MRI. *Imaging* **2**, 341–355 (2010).
15. Andersson, J.L.R., Skare, S. & Ashburner, J. How to correct susceptibility distortions in spin-echo echo-planar images: application to diffusion tensor imaging. *Neuroimage* **20**, 870–888 (2003).
16. Alexander, A.L., Tsuruda, J.S. & Parker, D.L. Elimination of eddy current artifacts in diffusion-weighted echo-planar images: the use of bipolar gradients. *Magn. Reson. Med.* **38**, 1016–1021 (1997).
17. Haselgrove, J.C. & Moore, J.R. Correction for distortion of echo-planar images used to calculate the apparent diffusion coefficient. *Magn. Reson. Med.* **36**, 960–964 (1996).
18. Anderson, J. *et al.* A comprehensive Gaussian Process framework for correcting distortions and movements in diffusion images. in *Proceedings of the International Society for Magnetic Resonance in Medicine (ISMRM) 20th Annual Meeting and Exhibition* (Melbourne, 2012).

19. Sotiropoulos, S.N. *et al.* Effects of image reconstruction on fibre orientation mapping from multichannel diffusion MRI: reducing the noise floor using SENSE. *Magn. Reson. Med.* advance online publication, doi:10.1002/mrm.24623 (7 February 2013).
20. Leemans, A. & Jones, D.K. The B-matrix must be rotated when correcting for subject motion in DTI data. *Magn. Reson. Med.* **61**, 1336–1349 2009).
21. Seunarine, K. & Alexander, D. Multiple fibers: beyond the diffusion tensor. in *Diffusion MRI: From Quantitative Measurement to in vivo Neuroanatomy* (eds., Johansen-Berg, H. and Behrens, T.E.J.) 55–72 (Academic Press, 2009).
22. Basser, P.J., Mattiello, J. & LeBihan, D. Estimation of the effective self-diffusion tensor from the NMR spin echo. *J. Magn. Reson. B* **103**, 247–254 (1994).
23. Tuch, D.S. *et al.* High angular resolution diffusion imaging reveals intravoxel white matter fiber heterogeneity. *Magn. Reson. Med.* **48**, 577–582 (2002).
24. Wedeen, V.J., Hagmann, P., Tseng, W.Y., Reese, T.G. & Weisskoff, R.M. Mapping complex tissue architecture with diffusion spectrum magnetic resonance imaging. *Magn. Reson. Med.* **54**, 1377–1386 (2005).
25. Behrens, T.E., Berg, H.J., Jbabdi, S., Rushworth, M.F. & Woolrich, M.W. Probabilistic diffusion tractography with multiple fibre orientations: What can we gain? *Neuroimage* **34**, 144–155 (2007).
26. Catani, M., Howard, R.J., Pajevic, S. & Jones, D.K. Virtual *in vivo* interactive dissection of white matter fasciculi in the human brain. *Neuroimage* **17**, 77–94 (2002).
27. Jbabdi, S. & Johansen-Berg, H. Tractography: where do we go from here? *Brain Connect.* **1**, 169–183 (2011).
28. Assaf, Y., Blumenfeld-Katzir, T., Yovel, Y. & Basser, P.J. AxCaliber: a method for measuring axon diameter distribution from diffusion MRI. *Magn. Reson. Med.* **59**, 1347–1354 (2008).
29. Jones, D.K., Knosche, T.R. & Turner, R. White matter integrity, fiber count, and other fallacies: The do's and don'ts of diffusion MRI. *Neuroimage* **73**, 239–254 (2013).
30. Mikula, S., Binding, J. & Denk, W. Staining and embedding the whole mouse brain for electron microscopy. *Nat. Methods* **9**, 1198–1201 (2012).
31. Behrens, T. & Jbabdi, S. MR diffusion tractography. in *Diffusion MRI: From Quantitative Measurement to in vivo Neuroanatomy* (eds., Johansen-Berg, H. and Behrens, T.E.J.) 333–352 (Academic Press, 2009).
32. Friston, K.J., Frith, C.D., Liddle, P.F. & Frackowiak, R.S. Functional connectivity: the principal-component analysis of large (PET) data sets. *J. Cereb. Blood Flow Metab.* **13**, 5–14 (1993).
33. Mennes, M., Kelly, C., Colcombe, S., Castellanos, F.X. & Milham, M.P. The extrinsic and intrinsic functional architectures of the human brain are not equivalent. *Cereb. Cortex* **23**, 223–229 (2013).
34. Biswal, B., Yetkin, F.Z., Haughton, V.M. & Hyde, J.S. Functional connectivity in the motor cortex of resting human brain using echo-planar MRI. *Magn. Reson. Med.* **34**, 537–541 (1995).
35. Toro, R., Fox, P.T. & Paus, T. Functional coactivation map of the human brain. *Cereb. Cortex* **18**, 2553–2559 (2008).
36. Chuang, K.-H. *et al.* Mapping resting-state functional connectivity using perfusion MRI. *Neuroimage* **40**, 1595–1605 (2008).
37. Ogawa, S. *et al.* Intrinsic signal changes accompanying sensory stimulation: functional brain mapping with magnetic resonance imaging. *Proc. Natl. Acad. Sci. USA* **89**, 5951–5955 (1992).
38. Wu, C.W. *et al.* Empirical evaluations of slice-timing, smoothing, and normalization effects in seed-based, resting-state functional magnetic resonance imaging analyses. *Brain Connect.* **1**, 401–410 (2011).
39. Friston, K.J. *et al.* Psychophysiological and modulatory interactions in neuroimaging. *Neuroimage* **6**, 218–229 (1997).
40. Friston, K.J., Williams, S., Howard, R., Frackowiak, R.S. & Turner, R. Movement-related effects in fMRI time-series. *Magn. Reson. Med.* **35**, 346–355 (1996).
41. Power, J.D., Barnes, K.A., Snyder, A.Z., Schlaggar, B.L. & Petersen, S.E. Spurious but systematic correlations in functional connectivity MRI networks arise from subject motion. *Neuroimage* **59**, 2142–2154 (2012).
42. Van Dijk, K.R.A., Sabuncu, M.R. & Buckner, R.L. The influence of head motion on intrinsic functional connectivity MRI. *Neuroimage* **59**, 431–438 (2012).
43. Satterthwaite, T.D. *et al.* Impact of in-scanner head motion on multiple measures of functional connectivity: Relevance for studies of neurodevelopment in youth. *Neuroimage* **60**, 623–632 (2012).
44. Satterthwaite, T.D. *et al.* An improved framework for confound regression and filtering for control of motion artifact in the preprocessing of resting-state functional connectivity data. *Neuroimage* **64**, 240–256 (2013).
45. Yan, C.G. *et al.* A comprehensive assessment of regional variation in the impact of head micromovements on functional connectomics. *Neuroimage* **76C**, 183–201 (2013).
46. Lund, T.E. fcMRI–mapping functional connectivity or correlating cardiac-induced noise? *Magn. Reson. Med.* **46**, 628–629 (2001).
47. Birn, R.M. The role of physiological noise in resting-state functional connectivity. *Neuroimage* **62**, 864–870 (2012).
48. Jo, H.J., Saad, Z.S., Simmons, W.K., Milbury, L.A. & Cox, R.W. Mapping sources of correlation in resting state fMRI, with artifact detection and removal. *Neuroimage* **52**, 571–582 (2010).
49. Perlbarg, V. *et al.* CORSICA: correction of structured noise in fMRI by automatic identification of ICA components. *Magn. Reson. Imaging* **25**, 35–46 (2007).
50. Fox, M.D., Zhang, D., Snyder, A.Z. & Raichle, M.E. The global signal and observed anticorrelated resting state brain networks. *J. Neurophysiol.* **101**, 3270–3283 (2009).
51. Murphy, K., Birn, R.M., Handwerker, D.a., Jones, T.B. & Bandettini, P.a. The impact of global signal regression on resting state correlations: are anti-correlated networks introduced? *Neuroimage* **44**, 893–905 (2009).
52. Saad, Z. *et al.* Trouble at rest: how correlation patterns and group differences become distorted after global signal regression. *Brain Connect.* **2**, 25–32 (2012).
53. Schölvinck, M.L., Maier, A., Ye, F.Q., Duyn, J.H. & Leopold, D.A. Neural basis of global resting-state fMRI activity. *Proc. Natl. Acad. Sci. USA* **107**, 10238–10243 (2010).
54. Cordes, D. *et al.* Frequencies contributing to functional connectivity in the cerebral cortex in "resting-state" data. *AJNR Am. J. Neuroradiol.* **22**, 1326–1333 (2001).
55. Niazy, R.K., Xie, J., Miller, K., Beckmann, C.F. & Smith, S.M. Spectral characteristics of resting state networks. *Prog. Brain Res.* **193**, 259–276 (2011).
56. Worsley, K.J., Marrett, S., Neelin, P. & Evans, A.C. Searching scale space for activation in PET images. *Hum. Brain Mapp.* **4**, 74–90 (1996).
57. Marrelec, G. *et al.* Regions, systems, and the brain: hierarchical measures of functional integration in fMRI. *Med. Image Anal.* **12**, 484–496 (2008).
58. Friston, K.J. & Frith, C.D. Time dependent changes in effective connectivity measured with PET. *Hum. Brain Mapp.* **1**, 69–79 (1993).
59. Smith, S.M. *et al.* Network modelling methods for fMRI. *Neuroimage* **54**, 875–891 (2011).
60. Varoquaux, G., Gramfort, A. & Poline, J.B. *Advances in Neural Information Processing Systems*. (Vancouver, Canada, 2010).
61. Marrelec, G. *et al.* Partial correlation for functional brain interactivity investigation in functional MRI. *Neuroimage* **32**, 228–237 (2006).
62. Varoquaux, G. *et al.* A group model for stable multi-subject ICA on fMRI datasets. *Neuroimage* **51**, 288–299 (2010).
63. Lowe, M.J., Dzemidzic, M., Lurito, J.T., Mathews, V.P. & Phillips, M.D. Correlations in low-frequency BOLD fluctuations reflect cortico-cortical connections. *Neuroimage* **12**, 582–587 (2000).
64. Sun, F.T., Miller, L.M. & D'Esposito, M. Measuring interregional functional connectivity using coherence and partial coherence analyses of fMRI data. *Neuroimage* **21**, 647–658 (2004).
65. Rissman, J., Gazzaley, A. & D'Esposito, M. Measuring functional connectivity during distinct stages of a cognitive task. *Neuroimage* **23**, 752–763 (2004).
66. Patel, R.S., Bowman, F.D. & Rilling, J.K. A Bayesian approach to determining connectivity of the human brain. *Hum. Brain Mapp.* **27**, 267–276 (2006).
67. Smith, S.M. *et al.* Correspondence of the brain's functional architecture during activation and rest. *Proc. Natl. Acad. Sci. USA* **106**, 13040–13045 (2009).
68. Peltier, S.J., Polk, T.A. & Noll, D.C. Detecting low-frequency functional connectivity in fMRI using a self-organizing map (SOM) algorithm. *Hum. Brain Mapp.* **20**, 220–226 (2003).
69. van den Heuvel, M., Mandl, R. & Hulshoff Pol, H. Normalized cut group clustering of resting-state fMRI data. *PLoS ONE* **3**, e2001 (2008).
70. Beckmann, C.F. Modelling with independent components. *Neuroimage* **62**, 891–901 (2012).
71. Breakspear, M., Brammer, M.J., Bullmore, E.T., Das, P. & Williams, L.M. Spatiotemporal wavelet resampling for functional neuroimaging data. *Hum. Brain Mapp.* **23**, 1–25 (2004).
72. Bellec, P., Marrelec, G. & Benali, H. A bootstrap test to investigate changes in brain connectivity for functional MRI. *Stat. Sin.* **18**, 1253–1268 (2008).

73. Smith, S.M. *et al.* Temporally-independent functional modes of spontaneous brain activity. *Proc. Natl. Acad. Sci. USA* **109**, 3131–3136 (2012).
74. Waites, A.B., Stanislavsky, A., Abbott, D.F. & Jackson, G.D. Effect of prior cognitive state on resting state networks measured with functional connectivity. *Hum. Brain Mapp.* **24**, 59–68 (2005).
75. Stevens, W.D., Buckner, R.L. & Schacter, D.L. Correlated low-frequency BOLD fluctuations in the resting human brain are modulated by recent experience in category-preferential visual regions. *Cereb. Cortex* **20**, 1997–2006 (2010).
76. Klingner, C.M., Hasler, C., Brodoehl, S., Axer, H. & Witte, O.W. Perceptual plasticity is mediated by connectivity changes of the medial thalamic nucleus. *Hum. Brain Mapp.* advance online publication, doi:10.1002/hbm.22074 (25 March 2012).
77. Riedl, V. *et al.* Repeated pain induces adaptations of intrinsic brain activity to reflect past and predict future pain. *Neuroimage* **57**, 206–213 (2011).
78. Vercammen, A., Knegtering, H., Liemburg, E.J., den Boer, J.A. & Aleman, A. Functional connectivity of the temporo-parietal region in schizophrenia: effects of rTMS treatment of auditory hallucinations. *J. Psychiatr. Res.* **44**, 725–731 (2010).
79. Keeser, D. *et al.* Prefrontal transcranial direct current stimulation changes connectivity of resting-state networks during fMRI. *J. Neurosci.* **31**, 15284–15293 (2011).
80. Fox, M.D., Buckner, R.L., White, M.P., Greicius, M.D. & Pascual-Leone, A. Efficacy of transcranial magnetic stimulation targets for depression is related to intrinsic functional connectivity with the subgenual cingulate. *Biol. Psychiatry* **72**, 595–603 (2012).
81. Tambini, A., Ketz, N. & Davachi, L. Enhanced brain correlations during rest are related to memory for recent experiences. *Neuron* **65**, 280–290 (2010).
82. Lewis, C.M., Baldassarre, A., Committeri, G., Romani, G.L. & Corbetta, M. Learning sculpts the spontaneous activity of the resting human brain. *Proc. Natl. Acad. Sci. USA* **106**, 17558–17563 (2009).
83. Koyama, M.S. *et al.* Cortical signatures of dyslexia and remediation: an intrinsic functional connectivity approach. *PLoS ONE* **8**, e55454 (2013).
84. Varoquaux, G. & Craddock, R.C. Learning and comparing functional connectomes across subjects. *Neuroimage* advance online publication, doi:10.1016/j.neuroimage.2013.04.007 (11 April 2013).
85. Rubinov, M. & Sporns, O. Complex network measures of brain connectivity: uses and interpretations. *Neuroimage* **52**, 1059–1069 (2010).
86. Genovese, C.R., Lazar, N.A. & Nichols, T. Thresholding of statistical maps in functional neuroimaging using the false discovery rate. *Neuroimage* **15**, 870–878 (2002).
87. Efron, B. When should hypothesis testing problems be combined? *Ann. Appl. Stat.* **2**, 197–223 (2008).
88. Zalesky, A., Fornito, A. & Bullmore, E.T. Network-based statistic: identifying differences in brain networks. *Neuroimage* **53**, 1197–1207 (2010).
89. Hu, J.X., Zhao, H. & Zhou, H.H. False Discovery Rate Control With Groups. *J. Am. Stat. Assoc.* **105**, 1215–1227 (2010).
90. Craddock, R.C., Holtzheimer, P.E., Hu, X.P. & Mayberg, H.S. Disease state prediction from resting state functional connectivity. *Magn. Reson. Med.* **62**, 1619–1628 (2009).
91. Dosenbach, N.U.F. *et al.* Prediction of individual brain maturity using fMRI. *Science* **329**, 1358–1361 (2010).
92. Bunke, H. A graph distance metric based on the maximal common subgraph. *Pattern Recognit. Lett.* **19**, 255–259 (1998).
93. Bullmore, E. & Sporns, O. Complex brain networks: graph theoretical analysis of structural and functional systems. *Nat. Rev. Neurosci.* **10**, 186–198 (2009).
94. Bullmore, E.T. & Bassett, D.S. Brain graphs: graphical models of the human brain connectome. *Annu. Rev. Clin. Psychol.* **7**, 113–140 (2011).
95. Zuo, X.N. *et al.* Network centrality in the human functional connectome. *Cereb. Cortex* **22**, 1862–1875 (2012).
96. Bassett, D.S., Meyer-Lindenberg, A., Achard, S., Duke, T. & Bullmore, E. Adaptive reconfiguration of fractal small-world human brain functional networks. *Proc. Natl. Acad. Sci. USA* **103**, 19518–19523 (2006).
97. Richiardi, J., Eryilmaz, H., Schwartz, S., Vuilleumier, P. & Van De Ville, D. Decoding brain states from fMRI connectivity graphs. *Neuroimage* **56**, 616–626 (2011).
98. Hansen, L.K. Multivariate strategies in functional magnetic resonance imaging. *Brain Lang.* **102**, 186–191 (2007).
99. Hastie, T., Tibshirani, R. & Friedman, J. *The Elements of Statistical Learning* (Springer, 2001).
100. Zhu, C.Z. *et al.* Discriminative analysis of brain function at resting-state for attention-deficit/hyperactivity disorder. *Med. Image Comput. Comput. Assist. Interv.* **8**, 468–475 (2005).
101. Vincent, J.L. *et al.* Intrinsic functional architecture in the anaesthetized monkey brain. *Nature* **447**, 83–86 (2007).
102. Pawela, C.P. *et al.* Resting-state functional connectivity of the rat brain. *Magn. Reson. Med.* **59**, 1021–1029 (2008).
103. Becerra, L., Pendse, G., Chang, P.-C., Bishop, J. & Borsook, D. Robust reproducible resting state networks in the awake rodent brain. *PLoS ONE* **6**, e25701 (2011).
104. Wang, K. *et al.* Temporal scaling properties and spatial synchronization of spontaneous blood oxygenation level-dependent (BOLD) signal fluctuations in rat sensorimotor network at different levels of isoflurane anesthesia. *NMR Biomed.* **24**, 61–67 (2011).
105. Pawela, C.P. *et al.* A protocol for use of medetomidine anesthesia in rats for extended studies using task-induced BOLD contrast and resting-state functional connectivity. *Neuroimage* **46**, 1137–1147 (2009).
106. Sörös, P. & Stanton, S.G. On variability and genes: inter-individual differences in auditory brain function. *Front. Hum. Neurosci.* **6**, 150 (2012).
107. Kapur, S., Phillips, A.G. & Insel, T.R. Why has it taken so long for biological psychiatry to develop clinical tests and what to do about it? *Mol. Psychiatry* **17**, 1174–1179 (2012).
108. Mennes, M., Biswal, B.B., Castellanos, F.X. & Milham, M.P. Making data sharing work: the FCP/INDI experience. *Neuroimage* advance online publication, doi:10.1016/j.neuroimage.2012.10.064 (30 October 2012).
109. Tzourio-Mazoyer, N. *et al.* Automated anatomical labeling of activations in SPM using a macroscopic anatomical parcellation of the MNI MRI single-subject brain. *Neuroimage* **15**, 273–289 (2002).
110. Desikan, R.S. *et al.* An automated labeling system for subdividing the human cerebral cortex on MRI scans into gyral based regions of interest. *Neuroimage* **31**, 968–980 (2006).
111. Eickhoff, S.B. *et al.* A new SPM toolbox for combining probabilistic cytoarchitectonic maps and functional imaging data. *Neuroimage* **25**, 1325–1335 (2005).
112. Lancaster, J.L. *et al.* Automated Talairach atlas labels for functional brain mapping. *Hum. Brain Mapp.* **10**, 120–131 (2000).
113. Margulies, D.S. *et al.* Precuneus shares intrinsic functional architecture in humans and monkeys. *Proc. Natl. Acad. Sci. USA* **106**, 20069–20074 (2009).
114. Knock, S.A. *et al.* The effects of physiologically plausible connectivity structure on local and global dynamics in large scale brain models. *J. Neurosci. Methods* **183**, 86–94 (2009).
115. Van Horn, J.D. *et al.* Mapping connectivity damage in the case of Phineas Gage. *PLoS ONE* **7**, e37454 (2012).
116. Jiang, T. Brainnetome: a new -ome to understand the brain and its disorders. *Neuroimage* advance online publication, doi:10.1016/j.neuroimage.2013.04.002 (6 April 2013).
117. Haacke, E.M., Bornw, R.W., Thompson, M.R. & Venkatesan, R. *Magnetic Resonance Imaging: Physical Principles and Sequence Design* (Wiley-Liss, 1999).
118. Bernstein, M.A., King, K.F. & Zhou, X.J. *Handbook of MRI Pulse Sequences* (Academic Press, 2004).
119. Blaimer, M. *et al.* SMASH, SENSE, PILS, GRAPPA: how to choose the optimal method. *Top. Magn. Reson. Imaging* **15**, 223–236 (2004).
120. Yacoub, E. *et al.* Spin-echo fMRI in humans using high spatial resolutions and high magnetic fields. *Magn. Reson. Med.* **49**, 655–664 (2003).
121. Weiskopf, N., Hutton, C., Josephs, O. & Deichmann, R. Optimal EPI parameters for reduction of susceptibility-induced BOLD sensitivity losses: a whole-brain analysis at 3 T and 1.5 T. *Neuroimage* **33**, 493–504 (2006).
122. Glover, G.H. & Law, C.S. Spiral-in/out BOLD fMRI for increased SNR and reduced susceptibility artifacts. *Magn. Reson. Med.* **46**, 515–522 (2001).
123. Heberlein, K.A. & Hu, X. Simultaneous acquisition of gradient-echo and asymmetric spin-echo for single-shot z-shim: Z-SAGA. *Magn. Reson. Med.* **51**, 212–216 (2004).
124. Gonzalez-Castillo, J., Roopchansingh, V., Bandettini, P.A. & Bodurka, J. Physiological noise effects on the flip angle selection in BOLD fMRI. *Neuroimage* **54**, 2764–2778 (2011).
125. Grootoonk, S. *et al.* Characterization and correction of interpolation effects in the realignment of fMRI time series. *Neuroimage* **11**, 49–57 (2000).

126. Noll, D.C., Cohen, J.D., Meyer, C.H. & Schneider, W. Spiral K-space MR imaging of cortical activation. *J. Magn. Reson. Imaging* **5**, 49–56 (1995).
127. Rabrait, C. *et al.* High temporal resolution functional MRI using parallel echo volumar imaging. *J. Magn. Reson. Imaging* **27**, 744–753 (2008).
128. Moeller, S. *et al.* Multiband multislice GE-EPI at 7 tesla, with 16-fold acceleration using partial parallel imaging with application to high spatial and temporal whole-brain fMRI. *Magn. Reson. Med.* **63**, 1144–1153 (2010).
129. Setsompop, K. *et al.* Improving diffusion MRI using simultaneous multi-slice echo planar imaging. *Neuroimage* **63**, 569–580 (2012).
130. Feinberg, D.A. *et al.* Multiplexed echo planar imaging for sub-second whole brain FMRI and fast diffusion imaging. *PLoS ONE* **5**, e15710 (2010).
131. Bright, M.G. & Murphy, K. Removing motion and physiological artifacts from intrinsic BOLD fluctuations using short echo data. *Neuroimage* **64**, 526–537 (2013).
132. Heine, L. *et al.* Resting state networks and consciousness: alterations of multiple resting state network connectivity in physiological, pharmacological, and pathological consciousness States. *Front. Psychol.* **3**, 295 (2012).
133. Boly, M. *et al.* Brain connectivity in disorders of consciousness. *Brain Connect.* **2**, 1–10 (2012).
134. Horovitz, S.G. *et al.* Decoupling of the brain's default mode network during deep sleep. *Proc. Natl. Acad. Sci. USA* **106**, 11376–11381 (2009).
135. Spoormaker, V.I. *et al.* Development of a large-scale functional brain network during human non-rapid eye movement sleep. *J. Neurosci.* **30**, 11379–11387 (2010).
136. Friston, K. Dynamic causal modeling and Granger causality Comments on: the identification of interacting networks in the brain using fMRI: model selection, causality and deconvolution. *Neuroimage* **58**, 303–305 (2011).
137. David, O. *et al.* Identifying neural drivers with functional MRI: an electrophysiological validation. *PLoS Biol.* **6**, 2683–2697 (2008).
138. Scannell, J.W., Burns, G.A., Hilgetag, C.C., O'Neil, M.A. & Young, M.P. The connectional organization of the cortico-thalamic system of the cat. *Cereb. Cortex* **9**, 277–299 (1999).
139. Mclntosh, A.R. & Gonzalez-Lima, F. Structural equation modeling and its application to network analysis in functional brain imaging. *Hum. Brain Mapp.* **2**, 2–22 (1994).
140. Lohmann, G., Erfurth, K., Müller, K. & Turner, R. Critical comments on dynamic causal modelling. *Neuroimage* **59**, 2322–2329 (2012).
141. Zhuang, J., LaConte, S., Peltier, S., Zhang, K. & Hu, X. Connectivity exploration with structural equation modeling: an fMRI study of bimanual motor coordination. *Neuroimage* **25**, 462–470 (2005).
142. Goebel, R. Investigating directed cortical interactions in time-resolved fMRI data using vector autoregressive modeling and Granger causality mapping. *Magn. Reson. Imaging* **21**, 1251–1261 (2003).
143. Granger, C.W. Investigating causal relations by econometric models and cross-spectral methods. *Econometrica* **37**, 424–438 (1969).
144. Sridharan, D., Levitin, D.J. & Menon, V. A critical role for the right fronto-insular cortex in switching between central-executive and default-mode networks. *Proc. Natl. Acad. Sci. USA* **105**, 12569–12574 (2008).
145. Deshpande, G. & Hu, X. Investigating effective brain connectivity from fMRI data: past findings and current issues with reference to Granger causality analysis. *Brain Connect.* **2**, 235–245 (2012).
146. Johnston, J.M. *et al.* Loss of resting interhemispheric functional connectivity after complete section of the corpus callosum. *J. Neurosci.* **28**, 6453–6458 (2008).
147. Matsumoto, R. *et al.* Functional connectivity in the human language system: a cortico-cortical evoked potential study. *Brain* **127**, 2316–2330 (2004).
148. Bohning, D.E. *et al.* Echoplanar BOLD fMRI of brain activation induced by concurrent transcranial magnetic stimulation. *Invest. Radiol.* **33**, 336–340 (1998).
149. Ruff, C.C. *et al.* Distinct causal influences of parietal versus frontal areas on human visual cortex: evidence from concurrent TMS-fMRI. *Cereb. Cortex* **18**, 817–827 (2008).
150. Datta, A. *et al.* Gyri-precise head model of transcranial direct current stimulation: improved spatial focality using a ring electrode versus conventional rectangular pad. *Brain Stimulat.* **2**, 201–207 (2009).